JOURNAL OF GEOPHYSICAL RESEARCH, VOL. 103, NO. A1, PAGES 29–45, JANUARY 1, 1998

Polar observations of convection with northward interplanetary magnetic field at dayside high latitudes

N. C. Maynard,[1] W. J. Burke,[2] D. R. Weimer,[1] F. S. Mozer,[3] J. D. Scudder,[4] C. T. Russell,[5] W. K. Peterson,[6] and R. P. Lepping[7]

Abstract. This study of dayside electrodynamics provides a first view of quasi-dc electric fields measured by Polar at middle altitudes. Three high-latitude passes chosen for analysis, occurred while Polar was in the midday sector and the interplanetary magnetic field (IMF) maintained a steady northward orientation at clock angles near 40° in the Y_{GSM} - Z_{GSM} plane. At different times during the passes, Polar encountered electron and ion fluxes from the central plasma sheet (CPS), the boundary plasma sheet, the polar rain, and various magnetospheric boundary regions. Although electric fields measured within the boundary layers were highly variable, we derived average components of plasma convection. The results compare favorably with convection characteristics of four-cell patterns observed at ionospheric altitudes with northward IMF. We show that Polar encountered lobe cells of both positive and negative polarity in the early postnoon sector. The negative potential extends well into the prenoon sector. Inverse, energy-dispersed fluxes of He^{++} were detected in regions of sunward convection. Sunward convection extended into the region of polar rain north of the merging line's projection. The magnetic merging signatures indicate that the process is both time varying and patchy. Particle and field measurements are consistent with the afternoon, auroral convection cell closing in the low-latitude boundary layer, which extend many tens of R_E tailward of the dusk terminator. Taken in a larger context, the Polar measurements provide new insight concerning the evolution of high-latitude convection from distorted two-cell patterns at large IMF clock angles to four cells at low clock angles

1. Introduction

One of the principal scientific goals of the Polar mission is to expand understanding of the electrodynamic coupling between the interplanetary medium and the Earth's magnetosphere. This paper focuses on the analysis of particle and field measurements acquired during three high-latitude passes of Polar in the midday sector. In each of the selected periods the interplanetary magnetic field (IMF) maintained relatively steady northward orientations. In all cases, IMF B_Y was positive (dawn-to-dusk); however, its magnitude relative to IMF B_Z varied. Although the penetration of particles and electric fields into the magnetosphere during periods of northward IMF has been studied using a broad spectrum of ground- and space-based sensors, the results sometimes appear to be inconsistent.

The dayside magnetosphere quickly responds to polarity changes of IMF B_Y and/or B_Z. Within a few minutes (approximately an Alfvén travel time) of the changes reaching the magnetopause, characteristic optical [*Sandholt*, 1991; *Sandholt et al.*, 1996; *Murphree et al.*, 1990] and plasma convection signatures [*Clauer and Friis-Christensen*, 1986] appear in the ionospheric projection of the cusp. Global ionospheric convection patterns at high geomagnetic latitudes are not established until the IMF has remained northward for longer than a half hour. During the Antarctic summer, *Maezawa* [1976] observed magnetic perturbations whose explanation required sunward convection in the central polar cap. Electric and magnetic fields measured by the S3-2 [*Burke et al.*, 1979], Atmospheric Explorer [*Reiff and Heelis*, 1994] and MAGSAT [*Iijima and Shibaji*, 1984] satellites suggested that with IMF $B_Z > 0$ and $B_Y \approx 0$,

[1]Mission Research Corporation, Nashua, New Hampshire.
[2]Phillips Laboratory, Hanscom Air Force Base, Massachusetts.
[3]Space Science Laboratory, University of California, Berkeley.
[4]Department of Space Physics and Astronomy, University of Iowa, Iowa City.
[5]Institute for Geophysics and Planetary Physics, University of California, Los Angeles.
[6]Lockheed Martin Space Sciences Laboratory, Palo Alto, California.
[7]Goddard Space Flight Center, Greenbelt, Maryland.

Paper number 97JA02295.
0148-0227/98/97JA-02295$09.00

a four-cell convection patterns evolves. This convection pattern consists of two cells in the polar cap, whose polarity is opposite to the adjacent, standard negative potential (clockwise) afternoon and positive (counterclockwise) morning cells. The polar cap convection cells are driven by magnetic merging at the poleward boundary of the cusp [*Dungey*, 1961; *Russell*, 1972]. The residual, standard-polarity pair of cells at auroral latitudes are weak. *Burke et al.* [1979] suggested that they are driven by the low latitude boundary layer (LLBL) [*Eastman et al.*, 1976].

Heppner and Maynard [1987] showed that during periods of northward IMF in which B_Y had large values, electric fields measured by the DE 2 satellite were consistent with the existence of two standard-polarity convection cells at high latitudes. Although distorted in shape, flow (equipotential) lines had the same sense of rotation as those observed when IMF $B_Z < 0$, but with the axis of symmetry rotated far from the noon–midnight meridian. The same orbits used by *Heppner and Maynard* [1987] to infer the convection pattern with $B_Z > 0$ and $B_Y > 0$ were reexamined by *Burke et al.* [1994] using simultaneous measurements from the retarding potential analyzer [*Hanson et al.*, 1981] and electron spectrometer [*Winningham et al.*, 1981] on DE 2. These provided supplementary information about the directions of convection flow lines crossing DE 2 trajectories and about the source regions of precipitating electrons. They concluded that the afternoon (negative potential) cell rotates into the prenoon sector and consists of two parts: (1) equipotentials whose associated magnetic flux is always open, and (2) equipotentials whose associated flux is both open and closed. Equipotentials with circulating open flux are commonly referred to as lobe cells [*Reiff and Burch*, 1985]. In the cases studied by *Burke et al.* [1994] the lobe cells were embedded within the afternoon cell and had the same sense of rotation. Recently, *Greenwald et al.* [1995] reported SUPERDARN observations of the dayside convection pattern evolving from two distorted cells into four cells as IMF B_Y decreased in magnitude relative to B_Z. The observed evolution of dayside convection compared favorably with prediction of the empirical model of *Weimer* [1996].

Satellite passages through the dayside high-latitude ionosphere are marked by encounters with distinctive particle and field characteristics. *Newell et al.* [1991a, b] have identified the spectral properties of electrons and ions in the dayside ionosphere whose magnetospheric sources are the central plasma sheet (CPS), the LLBL, the cusp and the mantle. *Newell and Meng* [1992, 1994] have utilized the large DMSP data base to determine the probabilities of encountering these regions as functions of magnetic latitude and magnetic local time (MLT).

In energy versus time spectrograms the cusp is distinguished by intense fluxes of low-energy (<100 eV) electrons and energy-dispersed ions. The latter signature is a time-of-flight, velocity-filter effect. During periods of northward (southward) IMF, the highest energy ions are detected near the poleward (equatorward) boundary of cusp precipitation [*Reiff et al.*, 1980; *Burch et al.*, 1980]. *Maynard* [1985] showed that cusp entry is also marked by a significant increase in the level of low-frequency noise measured by electric field sensors. The rapid traversal of the cusp by satellites in low-altitude orbits only allows for the detection of waves in the Pc 1 band [*Maynard*, 1985; *Basinska et al.*, 1992]. Satellite crossings of the ionospheric projections of magnetopause merging sites are frequently marked by electromagnetic spikes at the equatorward [*Maynard et al.*, 1991] and poleward [*Basinska et al.*, 1992] boundaries of cusp precipitation during periods of southward and northward IMF, respectively. On larger scales, ionospheric plasma convection in the cusp has a sunward (poleward) component when the IMF has a northward (southward) component. The azimuthal component of convection is controlled by the polarity of IMF B_Y. Convection is westward in the northern hemispheric cusp when IMF $B_Y > 0$. The opposite polarity relationship maintains in the southern hemisphere cusp. Finally, we note that besides the large scale, region 1/region 2 systems, the dayside ionosphere is marked by cusp and mantle field-aligned current (FAC) systems, often referred to as region 0 [*Iijima and Potemra*, 1976; *Earlandson et al.*, 1988].

Empirical models for patterns of high-latitude potentials (convection) have been constructed for various solar wind/IMF conditions. These have been based on pattern recognition normalization technique using the DE2 data set [*Heppner and Maynard*, 1987] and average values from the large DMSP databases [*Rich and Hairston*, 1994]. Recently, *Weimer* [1995, 1996] has developed a technique which uses least squares fits of DE2 electric field data to spherical harmonics that also includes effects of the dipole tilt angle. Published representations of the modeled convection patterns appear to be quite complex, especially for periods with IMF $B_Z > 0$ and $|B_Y| \leq B_Z$. Multiple small cells evolve within larger convection cells. Similar patterns to those of Weimer have been derived by *Ruohoniemi and Greenwald* [1996] by fitting Goose Bay HF radar observations to spherical harmonics.

This paper extends a preliminary report, which was mostly based on Polar electric field measurements taken during two Polar orbits (N. C. Maynard et al., Dayside electrodynamics observed by Polar with northward IMF, submitted to *Geophysical Monograph Series*, 1997). Expanding the study in local time and IMF clock angle, we present electric/ magnetic field and particle measurements taken during three example Polar passes at dayside, high latitudes throughout which the IMF B_Z and B_Y were positive. Magnetic field mapping using the T96 model [*Tsyganenko*, 1996] and observed en-

ergies/pitch angles of different ion masses are used to improve identifications of the source regions for electrodynamic signatures detected by Polar. The following section contains brief descriptions of Polar sensors used in this study. The observations section describes particle and field measurements taken at middle altitudes by Polar on April 3, 8, and May 11, 1996. Interpretations of the Polar observations in terms of encounters with middle altitude projections of previously identified magnetospheric plasma regimes are presented in the final section. In one case we were able to compare Polar measurements with simultaneous plasma drift observations of global high-latitude convection by a Defense Meteorological Satellite Program (DMSP) satellite. The DMSP measurements confirm that Polar made direct measurements of a negative potential lobe cell that was part of a four-cell convection pattern.

2. Instrumentation

Polar was launched into a 90° inclination orbit from the Western Test Range at Vandenburg, California, on February 24, 1996. The initial orbital plane was in the early postnoon/midnight local time sectors. Apogee (above the northern Polar cap) and perigee are at geocentric distances of 9 and 1.8 R_E, respectively. The spacecraft is spin stabilized at 10 rpm, with its spin axis perpendicular to the orbital plane. The four instruments whose measurements are used in this study are the electric field instrument (EFI), the magnetic field experiment (MFE), the HYDRA electron/ion spectrometer and the torroidal imaging mass angel spectrometer (TIMAS). Comprehensive descriptions of these sensors are provided by *Harvey et al.* [1995], *Russell et al.* [1995], *Scudder et al.* [1995], and *Shelley et al.* [1995], respectively. Only brief summaries of their relevant capabilities are provided below.

EFI consists of three dipoles to measure vector electric fields from potential differences between three pairs of spherical sensors. Two of the pairs of sensors are held at separation distances of 100 and 130 m by wire booms that rotate in the spacecraft's spin plane. The third pair is held at a separation of 14 m by a pair of rigid booms, aligned with the spin axis. The two spin-plane components of the electric field are represented by the symbols E_{X-Y} and E_Z. E_{X-Y} is the component of the spin-plane electric field which is nearly parallel to the GSE (geocentric solar ecliptic) XY plane (the axis orientation is determined by when the spacecraft Sun sensor contacts the Sun). Its sense is positive whenever the unit vector has a component in the $-X_{GSE}$ direction. E_Z completes the spin plane vector and is positive toward the GSE north pole. The third component, called E_{56}, points along the spin axis, positive in the sense that completes an orthogonal, right-hand coordinate system. Thus with polar orbiting in the noon meridian, components of the vector (E_{X-Y}, E_Z, E_{56}) are positive in the ($-X_{GSE}$, $+Z_{GSE}$, $+Y_{GSE}$) directions. Figure 1 shows the Earth with the X_{GSE} direction out of the paper, the orbit plane, and the orientation of the above spacecraft coordinate system for April 8, 1996, at 1530 UT (data to be discussed below). Data are sampled at a rate of 40 s^{-1} by all three sensors. Corrections must be made for dc offsets and fields induced by the satellite's $-\mathbf{V_S} \times \mathbf{B}$ motion and by a transformation of the measurements into the corotating frame. In addition, to minimize magnetic wake effects due to low plasma densities at Polar altitudes, we eliminated data taken when dipole axes were within specified avoidance angles to the magnetic field. The remaining data were fit to sine functions. Optimal avoidance angles varied with plasma density. Spin-fit measurements are presented for E_{X-Y} and E_Z every 6 s.

Measurements by the short booms of E_{56} are contaminated by unknown levels of dc offsets. These have two major sources, asymmetries of the potential distribution

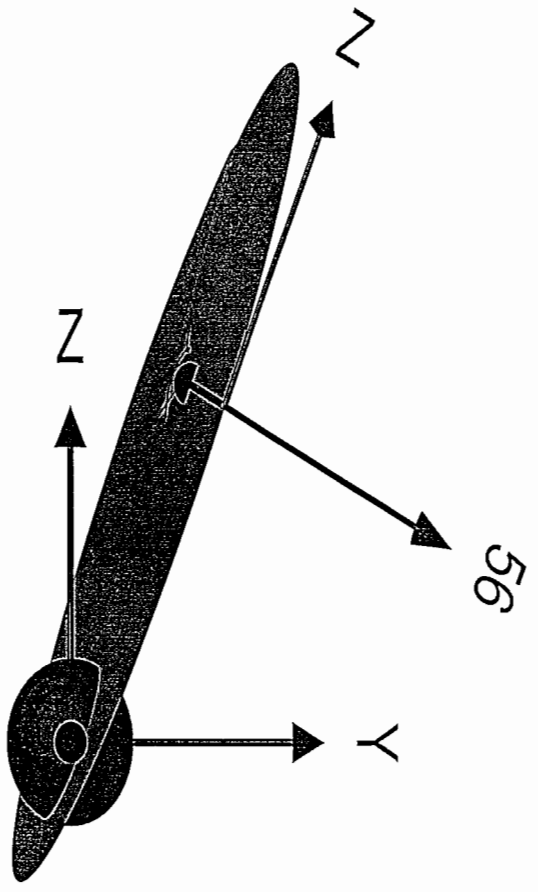

Figure 1. Sketch of the relationship of the $X-Y, Z, 56$ spacecraft coordinate system to GSE coordinates for April 8, 1996. The GSE coordinate system is centered at the Earth with X_{GSE} pointing out of the paper. The Polar orbit plane is shown with the spacecraft location and the orientation of the spacecraft system components for 1530 UT.

in the sheaths around the spacecraft and differences in the contact potentials of the two sensors. The first offset source occurs because the sensor elements are often embedded within the spacecraft sheath, to degrees that depend on the plasma density. To estimate these offsets and correct for them, we first subtract values that are proportional to the spacecraft potential. Residuals are then compared to estimates of the E_{56} component made using the assumption that $E \cdot B = 0$. Systematic deviations are then used to estimate the offset contribution due to differences in the surface contact potentials. Whenever magnetic field vectors lies very close the spin plane, the $E \cdot B = 0$ calculation amplifies small uncertainties about satellite attitude by large factors, creating large uncertainties in the calculated E_{56} value.

In some cases the dc offsets of measured E_{56} can be determined from comparisons with results at other times. For other cases, such as the two April passes, no reliable values of E_{56} could be determined. We also calculate the convective velocity ($\mathbf{V}$) using the onboard magnetic field measurements

$$\mathbf{V} = \frac{(\mathbf{E} \times \mathbf{B})}{B^2}$$

Our calculation of the V_{56} component of requires no knowledge of E_{56}.

MFI consists of two orthogonal, triaxial fluxgate magnetometers that are mounted on a nonconducting boom at separation distances from the nearest satellite surface of 5.97 m and 4.75 m. The outer sensor operates in two ranges ±5525 nT and ±694 nT; the inner sensor in the ranges ±46,700 nT and ±5860 nT. Data are sampled at a rate of 500 s^{-1} in all three components and averaged with a recursive filter to provide data at 100 and 8 samples s^{-1}. Only data sampled at the slower rate are available for this study. Here we are mostly concerned with magnetic perturbations produced by currents that couple the high-latitude to the magnetosphere or magnetosheath along closed or open magnetic field lines, respectively. Since these large-scale FAC systems generally extend much further in longitude than latitude [*Iijima and Potemra*, 1976], associated magnetic perturbations are mostly in the azimuthal component B_{56}. Positive-slope deflections in B_{56} with time (latitude) are detected as the northward moving Polar crosses FAC sheets directed into the ionosphere.

The HYDRA instrument consists of two pairs of electron and ion/electron spectrometers, each mounted 180° apart on the spacecraft body. In this paper we only use ion and electron measurements from the Duo Deca Electron Ion Spectrometer (DDEIS). As the name suggests, DDEIS is made up of six pairs of 127° electrostatic analyzers looking in different directions outward on a unit sphere. The electron spectrometer measures fluxes in the 1 eV to 10 keV range. The other spectrometer measures the fluxes of ions with energy per charge between 10 eV/q to 10 keV/ q, in 55 steps with a resolution in energy of $\delta E/E = 6\%$, and angle of 10° Fully three-dimensional distribution functions for electrons and ions are acquired in 0.5 s. To better represent the energies of in situ particles, we have adjusted the measured electron/ion count rates to reflect the effects of shifts induced by the floating potential of the spacecraft.

The TIMAS instrument uses a first-order, double focusing system of ion optics that simultaneously measures the spectral characteristics of positively charged ions in the mass per charge range 1 - 32 AMU e^{-1}, and energy per charge from 15 eV e^{-1} to 32 keV e^{-1} in 28 steps. Nearly the full 4π sr solid angle is swept out each half spin (3 s) of the satellite. In what follows we only display fluxes of He^{++} ions which primarily come from the solar wind. They provide tracers for identifying direct (cusp/mantle) and indirect (LLBL) paths from the magnetosheath to the locations of Polar.

3. Observations

This section presents particles and fields measured by Polar during three dayside passes in April and May of 1996. In all cases the satellite was moving toward higher altitudes and northern-hemisphere latitudes. Interplanetary conditions monitored by the WIND satellite near the times of interest are summarized in Table 1. Here we list the X_{GSE} and Y_{GSE} locations of the satellite in R_E, the average solar wind speeds V_{SW} in kilometers per second, the three GSM components of the IMF in nanotesla, and the approximate time in minutes that it takes for a signal in the solar wind to propagate to the subsolar magnetopause. The solar wind speed was in the low-to-moderate range. Interplanetary conditions were relatively stable for the periods of interest on April 3 and 8. Since we are primarily interested in steady state responses of the magnetosphere, knowing exact propagation times between Wind and the Earth are not critical for interpreting these events. On May 11, Wind was near the dawn meridian, just outside the bow shock. The IMF clock angle was gradually increasing

Table 1. Interplanetary Conditions

Date	X_{GSE}	Y_{GSE}	V_{SW}	B_X	B_Y	B_Z	Lag Time
April 3, 1996	77	2	353	-0.3 ±0.5	3.1 ±0.8	5.1 ±1.0	25
April 8, 1996	82	28	312	-1.0 ±0.8	6.4 ±0.5	6.8 ±0.4	29
May 11, 1996	2	-29	300[a]	4.8 ±0.4	1.9 ±0.7	3.0 ±0.5	0

[a]Assumed value based on later measurements.

with the nominal value near 35°. Approximate propagation times used for selecting the appropriate Wind data are given in Table 1. In all three cases the IMF had positive Y_{GSM} and Z_{GSM} components, and the IMF clock angle in the $Y - Z_{GSM}$ plane was near or less than 40°. We note that the level of geomagnetic activity was relatively low during the times of interest, with K_P indices of 2-, 2, and 2, respectively.

The remainder of this section presents Polar observations for each of the events starting with April 8. Here our task is to present physical quantities measured by the three sensors and point out empirical relationships between them. Interpretations, especially of potentially controversial aspects, are relegated to the discussion section. Because of their greater familiarity for identifying source regions, we show HYDRA and TIMAS measurements before those from EFI/MFE.

3.1. April 8, 1996

Plate 1 contains directional differential fluxes (cm^2 s sr keV/ e)$^{-1}$ of He^{++} (top) and omnidirectional count rates of electrons (middle) and ions (bottom) acquired between 1430 and 1730 on April 8, 1996. The data are in standard energy versus time spectrogram formats. Color bars to the right of the spectrograms provide flux and count-rate magnitudes. The DDEIS spectra give averages of 72 measurements at the given energy steps, accumulated over 13.8-s intervals. The measurements are presented as functions of universal time (UT), invariant latitude (ILT), magnetic local time (MLT) and geocentric distance in R_E. Values of the ILT, determined using IGRF 95 are related to the magnetic L shell by the familiar relationship $ILT = cos^{-1}(1/\sqrt{L})$.

On a purely empirical basis, the particle measurements from April 8 divide into four time intervals. (1) Prior to 1500 UT the highest ion count rates were at energies in the 8 to 3 keV/e range. The energy of peak counts decreased with increasing ILT. Electron counts were high (> 100) at energies below 60 eV and low (< 10) at energies above 100 eV. Their sharp spectral cutoff suggests that low- energy population mostly consists of atmospheric photoelectrons [*Doering et al.*, 1976]. (2) The period between 1500 and 1505 UT is marked by a burst of electrons with energies between 200 eV and 2 keV. A similar increase in the flux of ions with $\sim$ 5 keV/e was detected simultaneously. (3) The third period extends from 1505 to 1540 UT and is marked by nearly constant fluxes of electrons with energies <200 eV and dynamic variations in the ion measurements. From about 1505 to 1515 UT the energies of highest ion counts decreased from 4 to 0.2 keV/e. With notable small-scale variations, average ion energies remained within 0.2 - 0.3 keV/e until 1526UT when they began to increase systematically to 2 keV/e at 1537 UT. Phenomenologically, we describe the changing ion spectral characteristics at 1501 – 1508 UT and 1526 – 1537 UT as "standard" and "inverse" ion dispersion events. He^{++} ions are observed starting near 1508 UT and are intense between 1515 and 1530 UT. The inverse dispersion between 1526 and 1537 is also seen. Fluxes of He^{++} ions are low everywhere outside of this region. (4) After 1540 UT, DDEIS detected electron fluxes whose intensities and energies were significantly reduced, and ion count rates near background levels. Based on experience with the spectral characteristics of ion and electron fluxes observed at low altitudes [*Newell et al.*, 1991a, b], we identify the source regions encountered by Polar during the first interval as the central plasma sheet (before 1500 UT) and during the fourth interval as the polar cap (after 1540 UT), respectively. Interpretation of the source regions for particles observed during the second and third segments is deferred.

Figure 2 shows the spin-plane components of the electric field, the electric potential distribution along the trajectory, the spin-axis component of the plasma drift

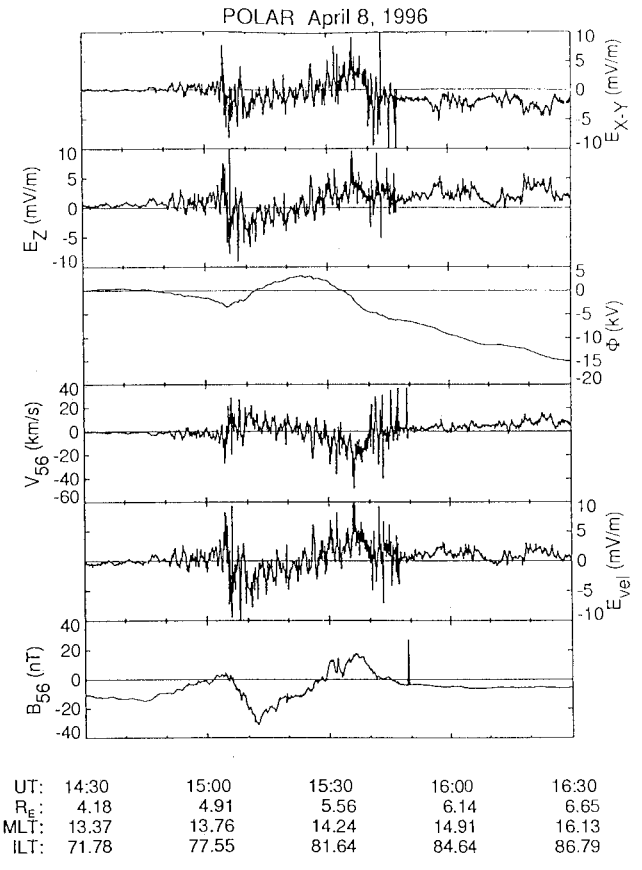

Figure 2. Electric and magnetic field measurements from 1430 to 1630 UT on April 8, 1996. From top to bottom the panels give the electric field spin-plane components E_{X-Y} and E_Z, the electric potential Φ derived from an integration along the Polar trajectory, the plasma-drift V_{56}, the electric field component in the spin plane along the velocity vector, and the difference between the measured magnetic field B_{56} component transverse to the orbital plane and the T96 model field component [*Tsyganenko*, 1996]. Four particle regions described in the text are marked at the bottom for reference.

V_{56}, the spin plane electric field component along the velocity vector, and magnetic field B_{56}, the latter with the T96 model field subtracted. A magnetic field avoidance angle of 0° up through 1550 UT and 45° thereafter was used for the electric field spin fits. Potential values are for the corotating reference frame for easy comparison to the ionospheric patterns. Since the satellite velocity $\mathbf{V_S}$ lies very close to the spin plane, estimates of the potential distribution along the trajectory

$$\Phi = \int -\mathbf{E} \cdot \mathbf{V_S}\, dt$$

should be accurate, despite our lack of knowledge about E_{56} for this pass. Its utility for understanding geomagnetic processes requires that the convection pattern be relatively steady over the interval in which the measurements were acquired. Note also that in interpreting variations in B_{56} as field-aligned currents we are assuming that changes of B are spatial and that large-scale temporal variations are small over the pass interval. The steady conditions observed by Wind in the interplanetary medium in this and the following case provides justification for this assumptions. For reference, we have marked the four different particle-flux segments at the bottom of Figure 2.

Attention is directed to the following seven points. (1) Prior to 1452 UT, the absolute values and variability of electric field was <1 mV/m. After this the amplitudes of variations grew. (2) From 1503 to 1542 UT the amplitude of electric field variations assumed values <5 mV/m. The periods of the variations ranged from a few tens of seconds to a few minutes (Pc 1 to Pc 4). (3) Average (quasi-dc) values of the electric field reverse polarity near 1525 UT, indicating a maximum in potential just prior to the beginning of the reverse dispersion event. (4) The third panel shows Polar crossed two regions of negative potential that bound a region of positive potential (1512 – 1534 UT). Viewed from above the north pole, the sense of rotation for plasma convection is clockwise/counterclockwise in regions of negative/positive potential (for instance, see patterns of *Heppner and Maynard* [1987]). In this case the potential of the counterclockwise rotating cell is ~3 kV. (5) The east-west component V_{56} had low values prior to 1504 UT. From 1504 to 1526 UT, Polar detected eastward flow (positive V_{56}), with an average value of ~10 km/s, as it crossed the region of standard ion dispersion and of low-energy, ions/electron fluxes. An average westward flow (negative V_{56}) of ~10 km/s marked the inverse dispersion event. This is consistent with counterclockwise plasma rotation in the cusp derived from Φ measurements. In the polar cap, V_{56} assumed low, steadily eastward values. (6) Variations in the trace of B_{56} mimic those of quasi-dc values of E_{X-Y} and E_Z. This indicates that Polar crossed several large-scale FAC sheets which close via Pedersen currents in the ionosphere [*Smiddy et al.*, 1980]. (7) Positive (negative) slopes in the B_{56} trace indicate FACs into (out of) the ionosphere. Consistent with a postnoon MLT trajectory, the positive (before 1505 UT) and negative (1505 – 1512 UT) slopes in B_{56} appear to be encounters with the afternoon region 2 and region 1 systems [*Iijima and Potemra*, 1976], respectively. The remaining FACs belong to the Region 0 system [*Erlandson*, 1988]. As expected, the main region 0 current has a polarity opposite to that of the adjacent region 1. A small region of upward current is seen poleward of the main region 0 current.

3.2. April 3, 1996

Plate 2 presents TIMAS and HYDRA measurements from 1200 to 1345 UT on April 3, 1996. Again, we divide the measurements as coming from four phenomenologically distinct regions. (1) Prior to ~1229 UT two populations of low- and high-energy electrons are sampled. From spectral similarities to fluxes detected at the same invariant latitudes during the previous pass, we identify them as photoelectrons and electrons from the CPS. Over the same period energetic (>1 keV) ion fluxes, whose mean energies decreased with increasing invariant latitude, were observed. (2) Fluxes of electrons with energies between about 500 eV and 4 keV underwent rapid increases and decreases at 1229 and 1238 UT, respectively. In this interval fluxes of ions with energies <200 eV rose above background. (3) From about 1238 to 1330 UT, Polar crossed a region of high fluxes of electrons whose mean energies, except for a few small-scale structures, decreased smoothly with invariant latitude. This region is marked by HYDRA observations of two ion populations with energies centered near 500 eV and 7 keV. TIMAS recorded three weak bursts of He^{++} ions with significant fluxes below 100 eV, at 1245, 1300, and 1315 UT. The peak energy of each burst is less than that of it predecessor. In all cases however the flux of He^{++} ions was nearly isotropic in pitch angle. (4) After 1330 UT, no He^{++} ions were detected and HYDRA measured polar rain electron and low ion flux levels, more typical of the polar cap. Again, we describe particles from the first and fourth intervals as marking the CPS and polar cap, respectively. Sources for particles of the second and third are discussed below.

Electric and magnetic field measurements from the same period are given in Figure 3. A magnetic field avoidance angle of 30° was used throughout for the electric field spin fits. We see that large-amplitude fluctuations in the electric field with periods near 10 s appear continuously between 1233 and 1300 UT, and in bursts near 1330 UT. The potential distribution detected by EFI, indicates that Polar was in a region of negative potential, characteristic of the afternoon convection cell. The plasma flow component $V_{56} = (E_{X-Y}B_Z - E_Z B_{X-Y})/B^2$ was weaker than observed on April 8, and after 1235 UT was predominantly toward the east. Large-scale variations with timescales of a few minutes or more in the spin-plane components of the electric field have a similar structure to those of the

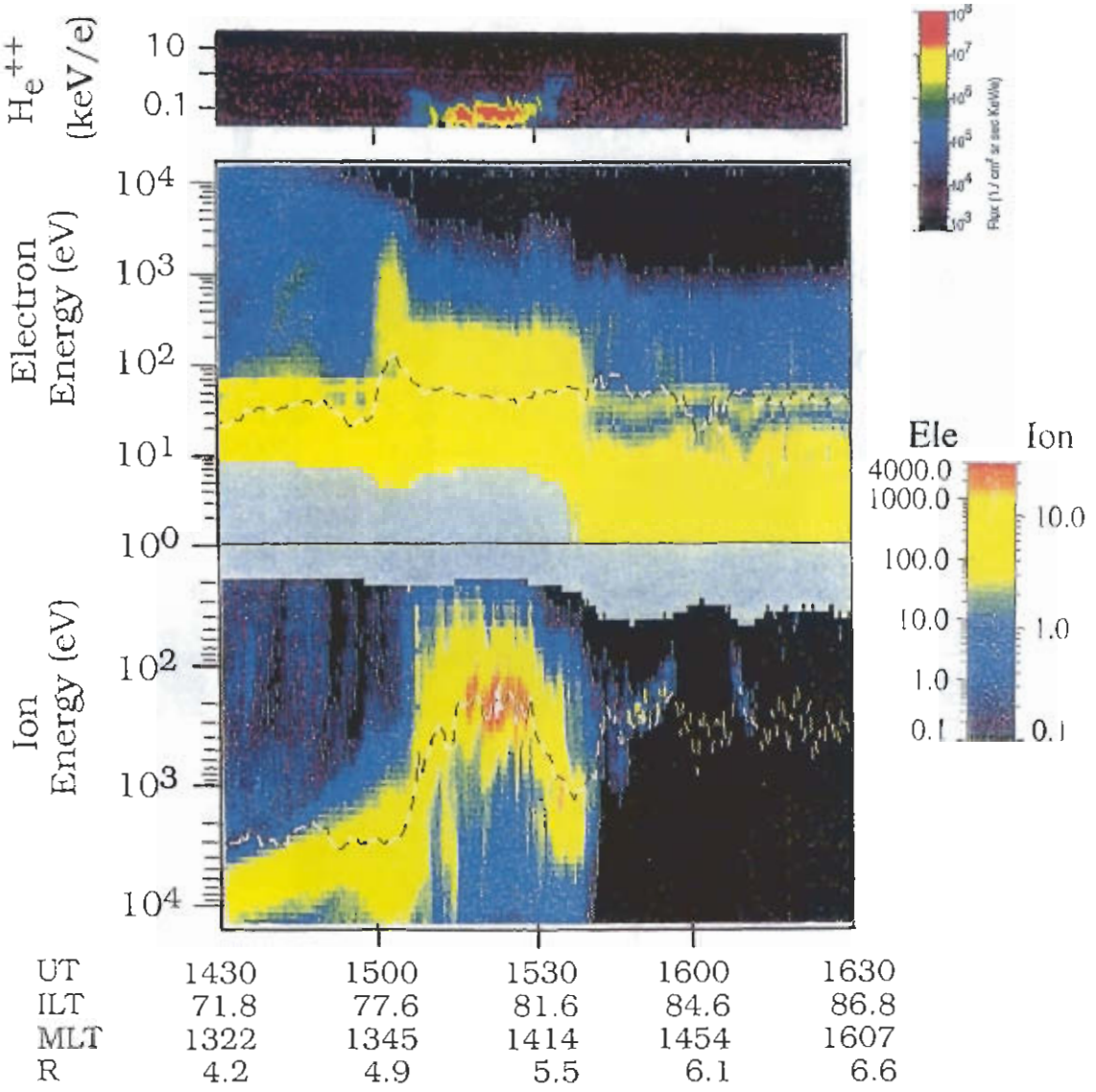

Plate 1. Particle measurements by TIMAS and HYDRA from 1430 to 1730 UT on April 8, 1996, in energy-versus time spectrograms. The top panel shows directional differential fluxes of He^{++} ions in number $(cm^2\ s\ sr\ keV/e)^{-1}$. Count rates for electrons with energies between 1 eV and 20 keV and ions with energies per charge between 10 eV/e and 20 keV/e are given in the middle and bottom panels, respectively. Note that the color-bar scales located to the right of the spectrograms, representing the intensities of measured quantities, are not the same for all plates. The dashed lines on HYDRA spectrograms give mean energies derived from distribution functions associated with observed count rates. We assume that the positive ions are H^+.

previous event, but are smaller in amplitude. They follow generally the large-scale variations of B_{56}, with the model field subtracted as in the April 8 event (note the bottom two panels). On large scale, the trace of B_{56} appears similar to that observed on April 8, but with smaller magnitude currents. Positive slopes, indicating FACs into the ionosphere were observed before 1236 UT (region 2) and from 1248 to 1308 UT; a negative trend in the slope of B_{56} (region 1) appeared between these intervals. A significant difference between the B_{56} traces of Figures 2 and 3 is the abundance of low-frequency fluctuations with amplitudes of a few nanoteslas. Their correlation with electric field variations indicates that Polar encountered Alfvén waves in the Pc 4 and 5 bands, as well as the large-scale FAC systems and suggests a more dynamic environment than that of the April 8 pass.

Finally, in regard to the variability, we note that the sharp negative turn in the B_{56} trace at 1300 UT coincides with a small-scale burst of electrons found in Plate 2, consistent with an upward current imbedded within the larger scale downward current.

3.3. May 11, 1996

On May 11, 1996, the IMF varied gradually and the Polar observations were more complex than on the two April days. Plate 3 presents TIMAS and HYDRA measurements taken between 1300 to 1400 UT. The Polar

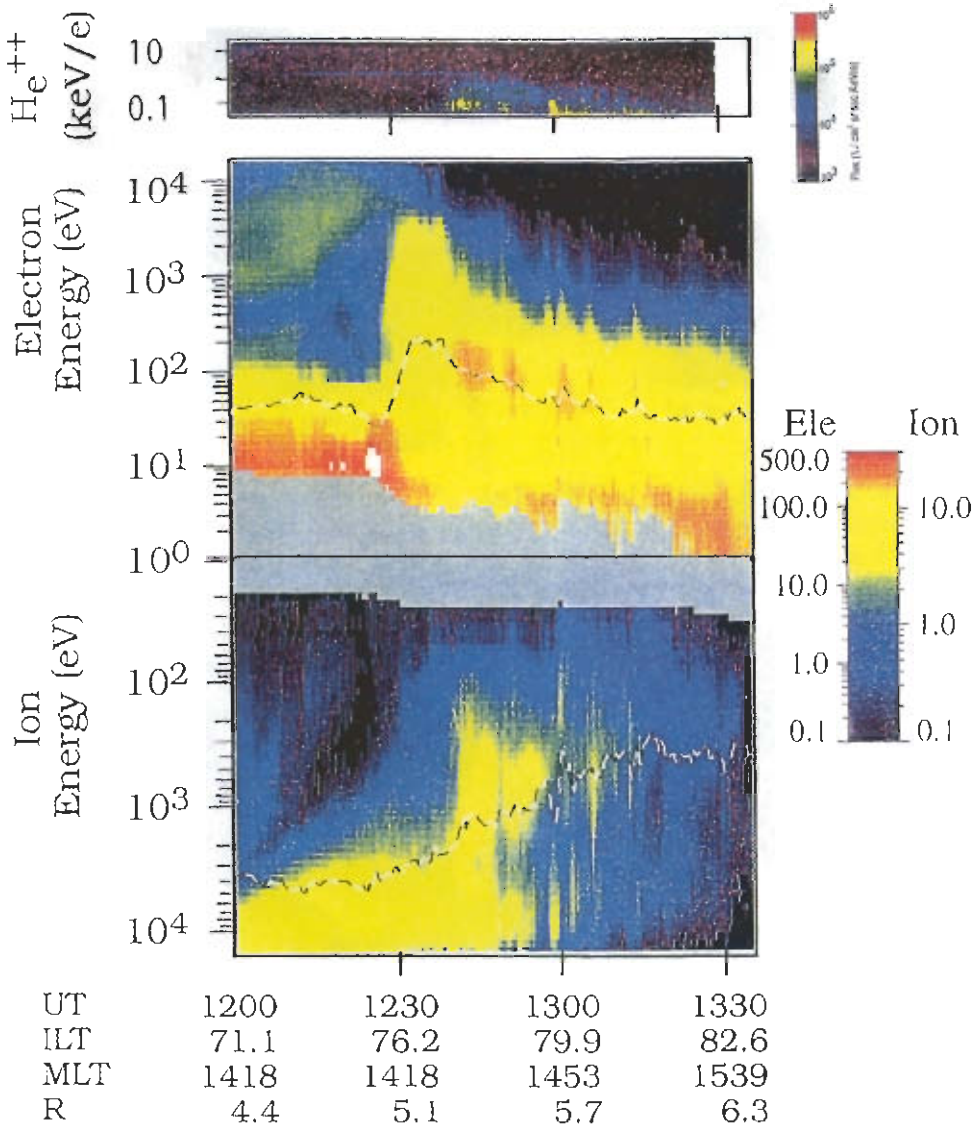

Plate 2. Spectrograms in the same format as in Plate 1 from 1100 to 1400 UT on April 3, 1996.

trajectory was very near magnetic noon (1133 to 1237 MLT) and at high invariant latitudes (78.6° to 85.0°). Examining first the HYDRA electron spectrogram, we see that there is no flux enhancement found at the transition between regions of high and low energy electron dominance as observed on the previous orbits. For this reason we divide the particles into three phenomenological segments. (1) Prior to 1311 UT, electron and ion fluxes observed by HYDRA were at high keV energies, characteristic of CPS fluxes. (2) The period between 1311 and 1344 UT is marked by complex variations whose characteristics we describe in more detail below. (3) After 1345 UT, HYDRA detected electron fluxes at polar rain levels. Ion fluxes during the first and third intervals were below the sensitivities of TIMAS and HYDRA.

The properties of particle measurements in the second interval change at 1330 UT. From 1311 to 1330 UT there were two forward ion dispersion signatures in the HYDRA spectrogram, 1312 through 1318 UT and 1319 through 1325 UT. Low-energy electron fluxes whose intensities gradually increased mark the interval. The flux of He^{++} ions ramped up after 1315 with their average energies increasing slightly at 1319 UT. The intensity underwent a step-like increase at 1324 UT.

The interval from 1330 to 1344 UT is characterized by multiple ion injections with reverse dispersion signatures. The electron flux was intense and contained two major enhancements in both intensity and energy at 1332 and 1340 UT. Intense He^{++} ion fluxes indicate access from the magnetosheath. The four peaks in ion energy with inverse dispersions observed by HYDRA at 1333, 1336, 1340, and 1344 UT have analogous features in the in the He^{++} spectrogram. We defer identification of source regions for the second interval to the discussion section.

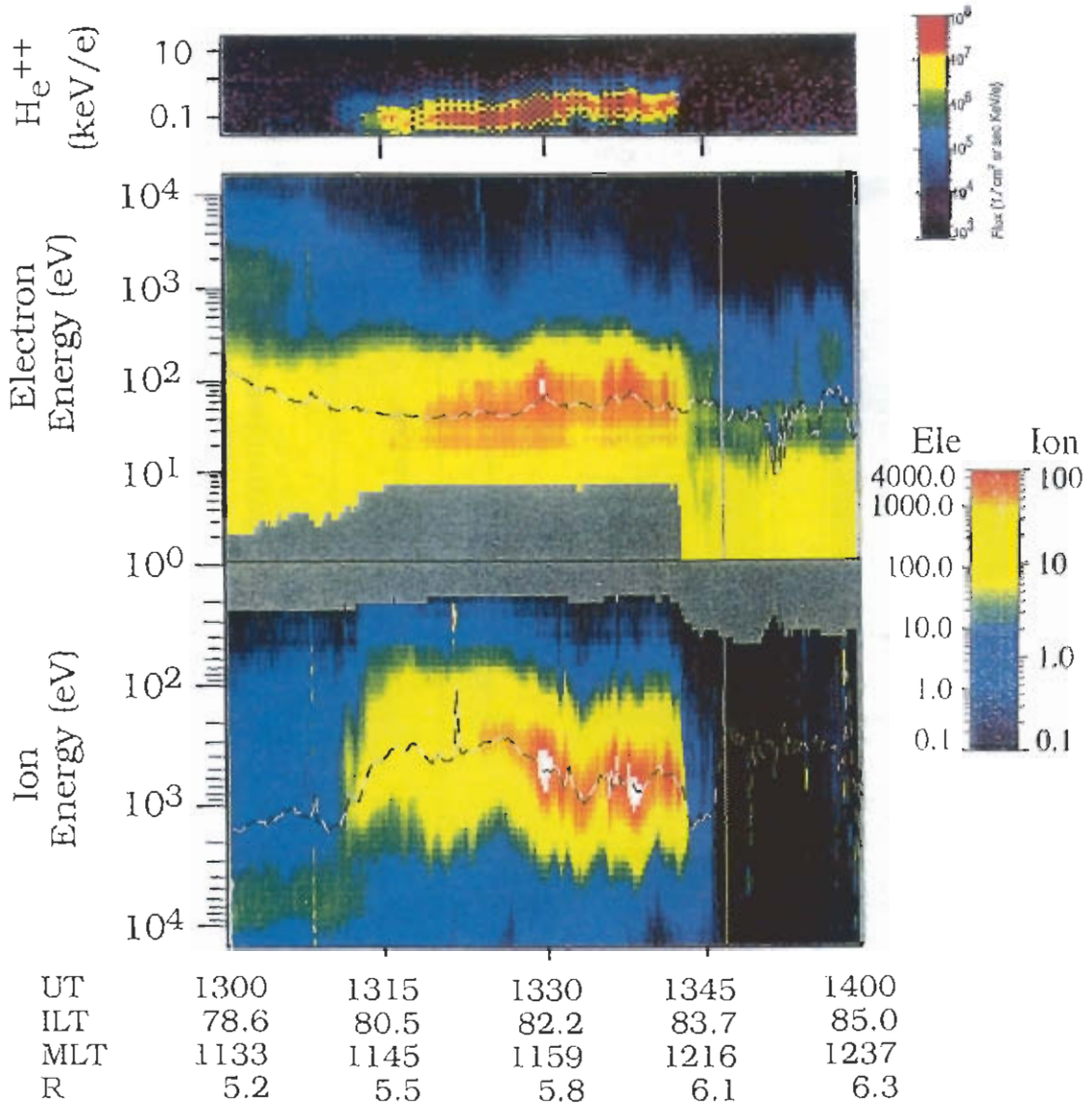

Plate 3. Spectrograms in the same format as in Plate 1 from 1300 to 1400 UT on May 11, 1996.

From top to bottom, Figure 4 presents the spin-plane components of the electric field, the potential distribution along the orbit track, the velocity components V_{X-Y} and V_{56} and the magnetic field component B_{56} with the T96 model field component subtracted. The inclusion of V_{X-Y} is possible because of a reasonable determination of the E_{56} offset could be made for this orbit. The magnetic field avoidance angles used were 30° through 1315 UT, 0° from 1315 to 1342 UT, and 60° thereafter. The assumption that large scale variations of E are spatial is again made in calculating the potential variation. Because of the slowly varying IMF, some temporal effects are possible. Polar remained close to a zero equipotential line until 1342 UT. We have calculated the potential distributions in both inertial (solid line) and corotating (dashed line) coordinates. We also note that similar large scale variations of E and B are present. However, the electric field amplitudes are smaller than observed during the April passes. Seasonally increasing conductivity may be a factor. More likely, there are variations in B_{56} that represent fringe effects from several spatially limited FAC systems located in the vicinity of the orbit track [*Fung and Hoffman*, 1992]. The positive slope in the B_{56} trace ending at ~1311 UT corresponds to interval (1) in the particle data of Plate 3. The signified downward current appears in a narrow latitude band marked by a weak negative potential well. Its source is in the central plasma sheet, and probably coincides with the afternoon region 2 FAC.

The neighboring region 1 upward currents extend through the beginning of the second particle interval to 1319:30 UT. Positive values of V_{X-Y} at this time indicate that convection was antisunward (poleward).

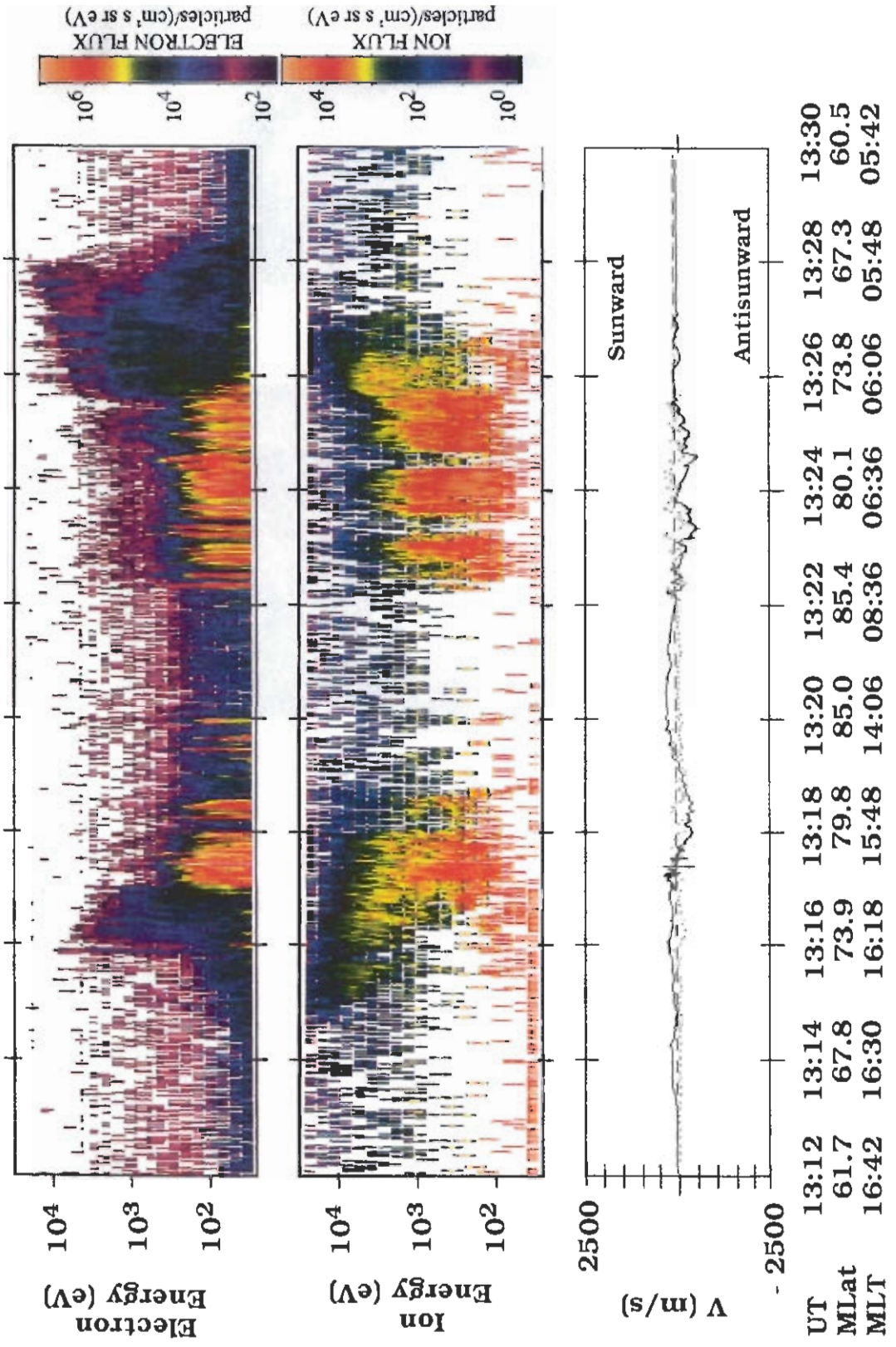

Plate 4. Directional differential fluxes of (top) electrons and (middle) ions measured by DMSP F13 between 1310 and 1330 UT on May 11, 1996. The trace in the bottom panel gives the cross-track component of plasma velocity measured by the drift meter on the spacecraft. It is positive in the sunward direction.

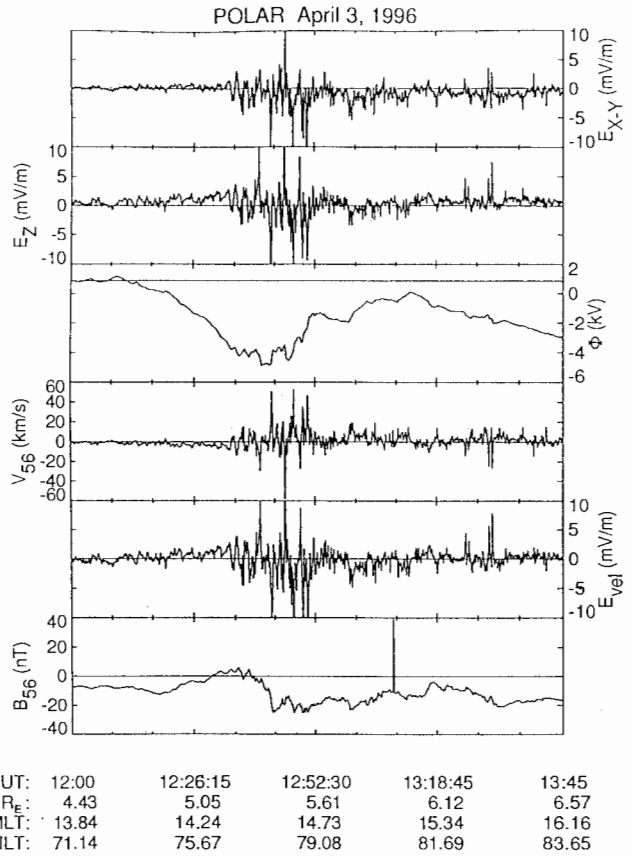

Figure 3. Electric and magnetic field measurements from 1200 to 1345 UT on April 3, 1996, in the same format as Figure 1.

V_{56} was initially toward dawn but reversed toward dusk near 1315 UT. From 1319:30 through 1330 UT the FAC polarity reversed, maintaining a nearly constant value. V_{56} again turned back toward dawn at 1323 UT. At this time V_{X-Y} turns sunward (equatorward) and remained so throughout the remainder of the pass. From 1319:30 through 1330 UT the potential had a slight positive excursion in the inertial system.

From 1330 to 1344 UT, particle and field patterns underwent further changes. A second relative maximum is seen in the potential pattern at 1336 UT. The potential then starts a negative trend which continues through the end of the pass. The inverse ion dispersions with energy peaks near 1333 and 1336 UT occurred in regions of eastward plasma drift ($V_{56} > 0$). The third and fourth inverse dispersions, noted in the discussion of Plate 3 are in regions of westward drift. Large sunward-velocity bursts accompany the first and third dispersions. Finally, we note that while the upward trend in the B_{56} trace continued through 1334 UT, the other magnetic field components had changes of similar magnitude, indicating that the satellite passed obliquely through FACs that may have been more filamentary than sheet-like in structure. After 1345 UT the principal plasma flow was sunward, and the potential became more negative as the satellite penetrated the polar cap.

4. Discussion

Data from these Polar passes with northward IMF exhibit both similarities and differences. The three events provide slices at different local times through dayside high latitudes under similar IMF clock angle conditions (~40°). While it is easy to identify the source regions for data acquired at the lowest and highest latitudes of the passes as the central plasma sheet and the polar cap, the three passes have very different properties in the intervening regions. Thus each pass provides different perspectives on dayside electrodynamics with northward IMF and the sources that drive the electrodynamics.

During the Polar passes of April 3 and 8, magnetic field variations showed the characteristic of the afternoon regions 2, 1 and 0 systems of FACs (downward/upward/downward) with an additional, small upward current at the poleward edge. At the highest and lowest invariant latitudes for which HYDRA spectral measurements are shown in Plates 1 and 2, one finds familiar characteristics of the CPS and polar cap. Localized bursts of kilovolt electrons are found in both instances near the poleward boundary of region 2 currents (interval 2 in each case). Since region 2 currents are driven by pressure gradients in the plasma sheet [*Harel et al.*, 1981], and particle spectral characteristics do not point elsewhere, we suggest that the bursts originate in the outer CPS. Physical processes responsible for the observed flux increases must operate deeper in the magnetosphere than the Polar orbit. The same current systems were observed during the May 11 pass. There was no burst of keV electrons at the high-latitude boundary of CPS fluxes, so that interval (1) encompassed the entire region 2 FAC.

The most intriguing aspects of the observations are in the intermediate latitude segments of the three cases (1505 – 1540 UT on April 8, 1238 – 1330 UT on April 3, and 1311 – 1344 UT on May 11). These times roughly span the regions 1 and 0 FACs and part of the upward FAC at the poleward edge. In all cases the segments of interest began as Polar entered the region 1 current sheet and ended as it entered the polar cap. Between these boundaries significantly different observations were made. Our analysis and interpretation of the observations from this portion of the Polar orbits follows for each case.

Figure 5a schematically represents the constraints that the data places on our interpretation of the convection pattern encountered by Polar on April 8, projected onto the ionosphere. From 1505 to 1512 UT the plasma had an eastward drift component and the ion spectrogram displayed a standard dispersion signature. During periods of southward IMF, such ion-dispersion

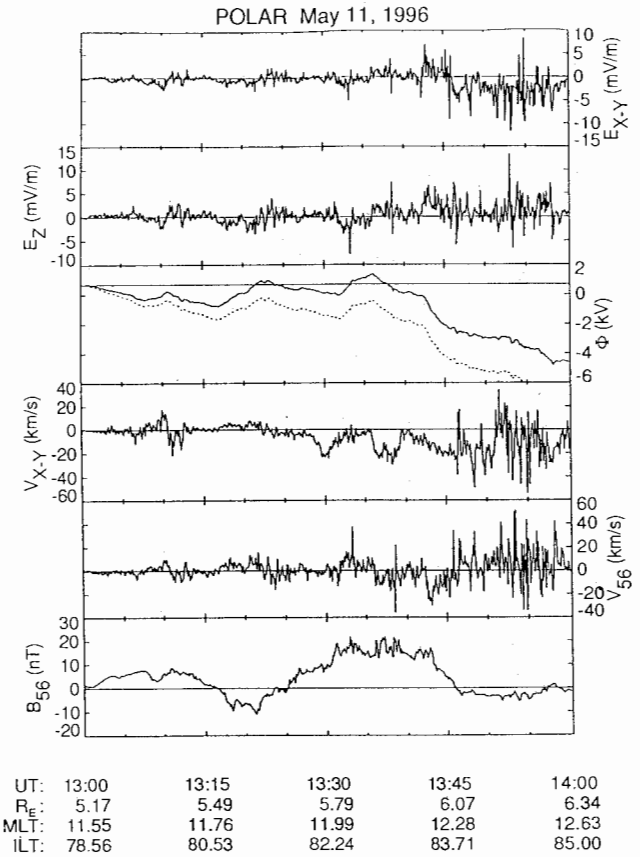

Figure 4. Electric and magnetic field measurements from 1300 – 1400 UT on May 11, 1996 in a format similar to Figure 1. Because E_{56} could be calculated during this orbit, we have included the plasma velocity component V_{X-Y}. It is positive when the plasma has an antisunward component of drift.

structures are normally regarded as time-of-flight effects as ions move from magnetic-merging sites on the magnetopause toward the ionosphere. With a northward IMF, the inner (low-latitude) portion of the LLBL is dominated by high-energy ions from the plasma sheet and the outer (high-latitude) portion by low-energy ions from the magnetosheath [*Eastman et al.*, 1976]. The apparent standard dispersion results from the superposition of these two populations. The separation of the two sources is even more evident in the second event (Plate 2). During the period of the apparent standard dispersion in Plate 1, Polar moved about 1.1° in invariant latitude. This is approximately the same latitudinal width of the LLBL observed above the ionosphere [*Smiddy et al.*, 1980]. An examination of the potential distribution measured between 1452 and 1512 UT, indicates that equipotentials in the CPS continue into the LLBL. Finally, our interpretation of the particles detected by HYDRA as coming from the LLBL is consistent with theoretical arguments developed by *Siscoe et al.* [1991] that the LLBL is the generator for the dayside region 1 currents.

From 1512 to 1537 UT on April 8, Polar crossed a positive potential cell in which plasma convection had an eastward (westward) drift component in its equatorward (poleward) parts. The inverse ion dispersion structure appeared in the poleward part. The simplest interpretation of these observations is that Polar went through the middle-altitude projection of the cusp. Magnetic merging with the northward IMF occurred at the cusp's poleward boundary. In this scenario, Polar crossed the magnetic mapping of the merging line (the heavy line in Figure 5a) where it encountered the highest energy ions of the inverse dispersion structure. After entering the polar cap, Polar again found itself in a region of negative potential. The question arises as to whether equipotentials with values >-2 kV in the polar cap connect with those in the LLBL. The answer appears to be no. From the Polar trajectory in Figure 5a, it is clear that plasma drifting along such equipotentials would have to move with a westward component. In fact, data in Figure 2 show that the plasma had an eastward drift component. For this reason we have represented the second negative potential cell as being made up of open flux circulating clockwise in the polar cap. HYDRA measurements of polar rain fluxes indicate that the satellite must have passed to the poleward side of this cell's merging line. The counterclockwise rotation of the first lobe cell is opposite to that of the normal afternoon convection cell and the embedded lobe cell observed by *Burke et al.* [1994]. It is similar to that observed by *Greenwald et al.* [1995]. We return to this point below. The FACs associated with this cell are the downward region 0 currents and upward current straddling the poleward edge.

Figure 5b sketches the data constraints on the convection directions in the pattern crossed by Polar on April 3, based on the potential distribution found in the third panel of Figure 3. There are two classes of equipotentials with westward drifting plasma in the region of CPS fluxes. Equipotentials crossed at the lowest latitudes are not intersected again by the orbit. At higher latitudes within the CPS, we find equipotentials that turn and are intersected for a second time between 1240 and 1330 UT as the potential increased from about

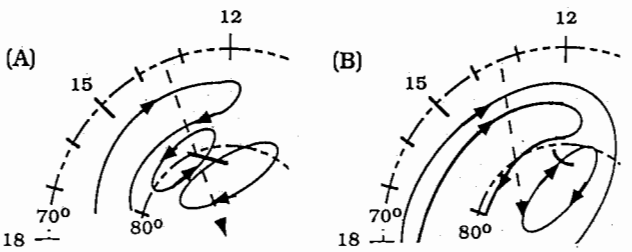

Figure 5. Schematic representation of ionospheric projection of potential distributions detected by Polar near 1515 UT on April 8, 1996, and 1300 UT on April 3, 1996. Directions of plasma flow are indicated by arrows.

-8 to -1.5 kV. It encompasses the region 1 and region 0 current systems and spans the invariant-latitude range 76.5° to 82.6°. Ion fluxes observed across the entire interval are generally weak with broad distributions in energy. In the equatorwardmost portion (1240 – 1255 UT) they appear bimodal in energy indicating that they are of LLBL origin [*Eastman et al.*, 1976].

Electric potential and particle measurements for April 3 are most simply explained if Polar remained within a projection of the boundary layer until it entered the polar cap. First, throughout the 1245 – 1330 UT period EFI measurements indicate that the plasma drift had an eastward component. During periods of IMF $B_Y > 0$, independent of the sign of IMF B_Z, magnetic tension forces on newly opened flux causes plasma to drift toward noon (west of the Polar orbit) then into the morningside of the polar cap. Thus the drift expected from merging is opposite to the observed eastward direction. The corresponding TIMAS data (Plate 2) shows three bursts of He^{++} ions in this region.

The observed fluxes must be coming from boundary layers of the magnetotail. To illustrate this, Figure 6 displays the projection of the Polar orbit at each of the times of the bursts of He^{++} ions (1245, 1300, and 1315 UT) using the T96 model. A nominal magnetopause is also shown. The particles enter the boundary layer from well behind the dusk terminator. All three are within a weak downward FAC poleward of the region 1 currents. Because of finite propagation times required to travel along the magnetic field lines to Polar and possible entry above the equatorial plane, the mapped position in the equatorial plane may be tailward of actual entry points in the boundary layer. However, the conclusion that Polar traversed the mapped boundary layer at points well behind the dusk terminator is clear. Second, electron and ion fluxes observed between 1255 and 1330 UT show gradual, rather than abrupt, transitions to polar cap levels. This is seen most clearly in the electrons, whose average energies monotonically decreased with increasing invariant latitude. It may be viewed as due to an adiabatic cooling of electrons as flux tubes grow in volume and convect down stream along the flank of the magnetotail. We have noted that each of the He^{++} bursts is lower energy than the one preceding it, characteristic of sources being at greater distances down the tail. Although the latitudinal width of the projection of this boundary layer is larger than expected, the potential drop of ~8 kV measured across the boundary layer is similar to those reported by *Smiddy et al.* [1980] and *Mozer* [1984].

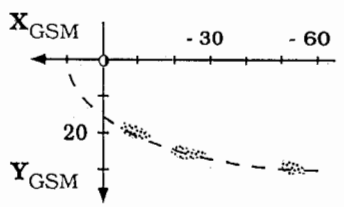

Figure 6. Schematic representation of the projection of the regions of He^{++} fluxes detected by Polar to the equatorial plane using the T96 magnetic field model.

The most complex particle and field variations were measured on May 11 as the Polar orbit straddles the noon magnetic meridian. Cusp/cleft signatures were encountered at unusually high magnetic latitudes [*Newell and Meng*, 1992, 1994]. We anticipate that the satellite's location mapped to several different geophysical regions over a small latitudinal span. Figure 7 is a three-dimensional (3-D) image of magnetic field lines crossed by the Polar trajectory at 5-min intervals. The T96 model with the prevailing DST value of -3 nT and appropriate solar wind conditions were used in the calculations. Until 1315 UT, the field lines mapped to the prenoon dayside boundary layer. The field line crossed at 1320 UT mapped to the dawn flank of the magnetotail, well behind the terminator. The remaining field lines map into the high latitude boundary of the magnetosphere. Since the T96 model is very sensitive to input conditions, the map can only be used as a qualitative guide; however, it provides useful guidance for interpreting the Polar measurements from this period.

The first part of the second interval (1311 to 1319:30 UT) includes all of the duskside region 1 currents and the first forward-dispersion ion event. We interpret this as part of the duskside convection cell because of its negative potential and the upward polarity FACs. However, the magnetic local time and mapping suggests a prenoon dayside boundary layer source.

The latter part of the second interval (1319:30 to 1330 UT) is within the downward region 0 currents and contains the second forward-dispersion ion event. These currents have the same polarity as dawnside region 1 currents. Figure 7 suggests that this second forward dispersion feature may be on field lines that are heading toward the dawn flank. He^{++} was present at this time. Plasma velocities are initially toward dusk and then reverse toward dawn. The potentials are all small and indicate that Polar was moving close to a zero equipotential line between two convection cells of opposite polarity.

Figure 7 suggests that Polar locations mapped to the cusp/mantle region during the latter part of the second interval. Here Polar crossed four injection structures with reverse dispersion characteristics which are regarded as signatures of magnetic merging poleward of the cusp. The azimuthal plasma velocity components of the first and second dispersion events were opposite to those of the third and fourth. This suggests that the merging sites on the magnetopause mapped to the east and west sides of the Polar trajectory. The sporadic nature of the particle and field measurements indicate that Polar encountered effects of temporally varying coupling between the magnetosphere and the interplanetary medium. This would take the form of time-dependent, patchy merging poleward of the cusp.

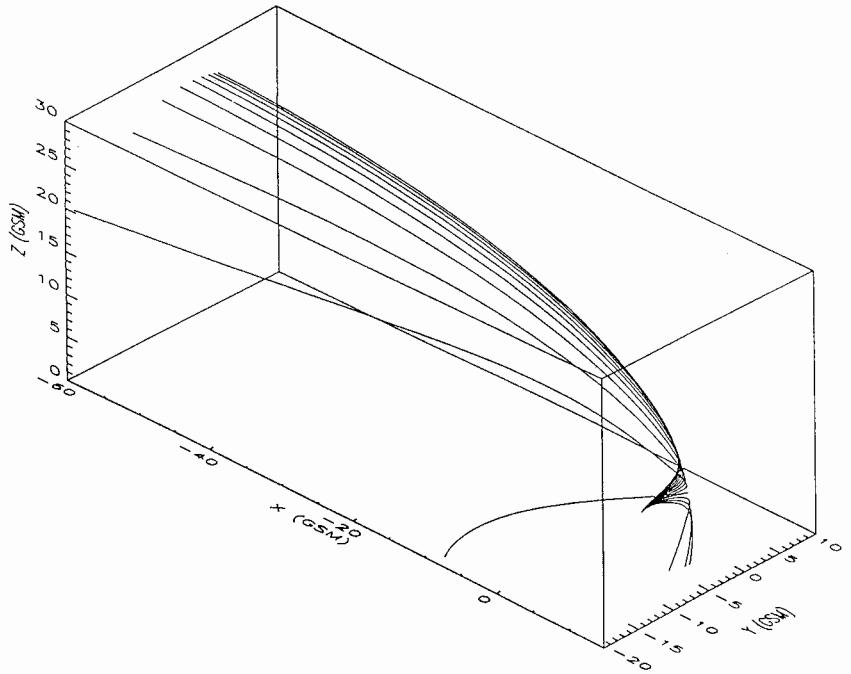

Figure 7. Three-dimensional projection of magnetic field lines crossed by Polar at 5 minute intervals from 1300 to 1400 on May 11, 1996, using the T96 magnetic field model.

The strong fluxes of He^{++} confirm that energetic particles had direct access from the magnetosheath. The potential turned more negative at the end of this interval and the trend continued into the region of polar rain fluxes. Significant parts of that cell must have extended into the prenoon sector.

To provide a larger context for the Polar measurements just discussed we have examined particle and plasma drift measurements (Plate 4) taken during a nearly simultaneous dusk to dawn pass made by the Defense Meteorological Satellite Program (DMSP F13). The horizontal (vertical) cross-track ion drift measurements presented as the solid blue (dotted red) trace in the lower panel show that convection was weak (<250 m/s) in the afternoon auroral oval, and unmeasurably small in the morning oval. This is consistent with results of *Heppner and Maynard* [1987], who showed that with IMF B_Y and $B_Z > 0$, the morning cell is confined to the predawn quadrant. We note the presence of stronger (~500 m/s) convection along the flanks of the polar cap and an extensive region of sunward convection in the central polar cap. These are the signatures of four-cell convection patterns of *Burke et al.* [1979]. Ephemeris data given beneath the plate indicate that DMSP F13 crossed the noon magnetic meridian at about 1321 UT and 85° magnetic latitude. Across the region of polar rain precipitation plasma convection had a steady sunward component. This is consistent with Polar measurements of sunward convection up to 85° near the noon meridian. Taken as a whole, the measurements from the two satellites suggest that the Polar trajectory carried it along the boundary between positive and negative potential lobe cells until 1345 UT when it entered the negative potential cell. The small potentials measured by Polar do not easily adapt to a strongly distorted two cell interpretation.

Synthesizing these three passes with $0 < B_Y < B_Z$ and similar IMF clock angles, solar wind particles had access to the high latitude magnetosphere along several different paths. In all of the Polar passes, HYDRA and TIMAS detected energy-dispersed ion signatures and He^{++} ion fluxes in regions that couple to the LLBL. Some of the dispersion signatures reflect superpositions of plasma sheet and magnetosheath populations; others from adiabatic cooling in flux tubes with expanding volumes. During the April 3 event, He^{++} ions entered the boundary layer on the flank of the magnetotail well behind the dusk terminator. The April 8 and May 11 passes provide evidence for the existence of negative potential lobe cells that extend into the prenoon MLT sector. On April 8 a small, positive-potential lobe cell was observed in the early postnoon sector. DMSP F13 measurements show that such a cell was also present at the time of the May 11 pass. Figure 8 presents our empirical synthesis of the convection patterns encountered on the three Polar passes. It is critical that these not be regarded as static. Magnetic merging that drives the cells can be both temporally and spatially varying.

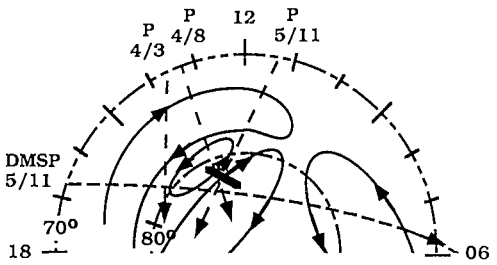

Figure 8. Schematic representation of high-latitude convection/potential patterns encountered by Polar on April 3 and 8 and May 11, 1996. Approximate orbital traces relative to convection patterns for Polar and DMSP F13 are indicated for reference.

The afternoon boundary layer driven cell can extend into the prenoon sector. DMSP measurements indicate that little of the morning side convection cell extends sunward of the dawn terminator.

5. Summary

This study of dayside high-latitude electrodynamics based on Polar measurements, represents a first view of quasi-dc electric fields from middle altitudes. Comparisons of the measurements with those made at lower altitudes not only increase confidence that EFI operated as intended, but they also provide new insight on how convection patterns evolve with changing IMF clock angles and about the source regions for particles reaching the satellite. The following conclusions, which either confirm or add to previous understanding, are derived from our analysis of Polar particle and field measurements with northward IMF and with $B_Y > 0$, augmented with DMSP and Wind data.

1. The center of a negative potential lobe cell, previously observed in the postnoon sector and embedded within the afternoon negative-potential cell for larger IMF clock angles [*Burke et al.*, 1994], is detected by Polar in the prenoon sector for clock angles ~40° and smaller.

2. A positive potential lobe cell evolves in the postnoon MLT sector as the IMF clock angle decreases.

3. The emergence of the positive-potential lobe cell in the postnoon sector and the movement of the negative-potential lobe cell to prenoon local times as the IMF clock angle decreases below 35°, describes the manner in which distorted two-cell convection patterns at large IMF clock angles evolve to three or four-cell patterns. Two lobe cells of polarity opposite to the normal convection pattern are needed for consistency with the NBZ currents observed with IMF clock angles near zero.

4. The reverse energy versus time ion dispersions on the poleward edge of the cusp, observed on April 8 and May 11, are signatures of merging that drives lobe-cell convection.

5. Significant, isotropic fluxes of He^{++} ions demonstrate that particles on newly merged field lines have direct access from the magnetosheath.

6. The magnetic merging that drives lobe cells may be patchy and/or vary with time.

7. Forward-dispersion ion signatures detected near the equatorward edge of magnetosheath like fluxes have sources in the LLBL. Some entry occurs on the dawnside of noon and/or tailward of the terminator.

8. He^{++} ion fluxes were detected on field lines that map to the equatorial distances tens of R_E down the dusk flank of the magnetotail (Figure 6). A similar entry source may be inferred along the dawn flank (Figure 7).

Acknowledgments. This work was performed under funding from the NASA GGS Program (part of the International Solar Terrestrial Physics Program). Work at UC Berkeley and Mission Research Corporation was supported under contract number NAS5-30367 and grant number NAG5-3182. Work at UCLA was supported under grant number NAG5-3171. Work at Iowa was supported under grant NAG S-2231. W.K.P. was supported by contract NAS5-33032. W.K.P. also thanks D. Baker and the staff of LASP for their kind hospitality. W.J.B. was supported in part by NASA and in part by the U.S. Air Force Office of Scientific Research task 2311PL014. We thank K. W. Ogilvie for the use of the Wind plasma data.

The Editor thanks R. A. Greenwald and another referee for their assistance in evaluating this paper.

References

Basinska, E. M., W. J. Burke, N. C. Maynard, W, J. Hughes, J. D. Winningham, and W. B. Hanson, Small-scale electrodynamics of the cusp with northward interplanetary magnetic field, *J. Geophys. Res., 97*, 6369, 1992.

Burch, J. L., P .H. Reiff, R. A. Heelis, R. W. Spiro, and S. A. Fields, Cusp region particle precipitation and ion convection for northward interplanetary field, *Geophys. Res. Lett., 7*, 393, 1980.

Burke, W. J., E. M. Basinska, N. C. Maynard, W. B. Hanson, J. P. Slavin, and J. D. Winningham, Polar cap potential distributions during periods of positive IMF B_Y and B_Z, *J. Atmos. Terres. Phys., 56*, 209, 1994.

Burke, W. J., M. C. Kelley, R. C. Sagalyn, M. Smiddy, and S. T. Lai, Polar cap electric field structures with northward interplanetary magnetic field, *Geophys. Res. Lett., 6*, 21, 1979.

Clauer, C. R., and E. Friis-Christensen, High-latitude electric fields and currents during strongly northward magnetic field: Observations and model simulations, *J. Geophys. Res., 91*, 6959, 1986.

Doering, J. P., W. K. Peterson, C. O. Bostrom, and T. A. Potemra, High resolution daytime photoelectron energy spectra from AE-E, *Geophys. Res. Lett.*, 3, 129, 1976.

Dungey, J. W., Interplanetary magnetic field and the auroral zones, *Phys. Rev. Lett., 6*, 47, 1961.

Eastman T. E., E. W. Hones Jr., S. J. Bame, and J. R. Asbridge, The magnetospheric boundary layer: Site of plasma, momentum and energy transfer from the magnetosheath into the magnetosphere, *Geophys. Res. Lett., 3*, 685, 1976.

Erlandson, R. E., L. J. Zanetti, T. A. Potemra, P. F. Bythrow, and R. Lundin, IMF B_Y dependence of region 1 Birkeland currents near noon, *J. Geophys. Res., 93*, 9804, 1988.

Fung, S. F., and R. A. Hoffman, Finite geometry of field-aligned currents, *J. Geophys. Res., 97*, 8569, 1992.

Greenwald, R. A., W. A. Bristow, G. J. Sofko, C. Senior, J.-C. Cerisier, and A. Szabo, Super dual auroral radar network radar imaging of dayside high-latitude convection under northward magnetic field: Toward resolving the distorted two-cell versus multicell controversy, *J. Geophys. Res., 100*, 19,661, 1995.

Hanson, W. B., R. A Heelis, R. A. Power, C. R. Lippincott, D. R. Zuccaro, B. J. Holt, L. H. Harmon, and S. Sanatani, The retarding potential analyzer for Dynamics Explorer-B, *Space Sci. Instrum., 5*, 503, 1981.

Harel, M., R. A. Wolf, P. H. Reiff, R. W. Spiro, W. J. Burke, F. J. Rich, and M. Smiddy, Quantitative simulation of a magnetospheric substorm 1. Model logic and overview, *J. Geophys. Res., 86*, 2217, 1981.

Harvey, P., F. S. Mozer, D. Pankow, J. Wygant, N. C. Maynard, H. Singer, W. Sullivan, P. B. Anderson, R. Pfaff, T. Aggson, A. Pedersen, C. -G. Fälthammer, and P. Tanskannen, The electric field instrument on the Polar satellite, in *The Global Geospace Mission*, edited by C. T. Russell, p. 583, Kluwer Acad., Norwell, Mass., 1995.

Heppner J.P., and N.C. Maynard, Empirical high-latitude electric field models, *J. Geophys. Res., 92*, 4467, 1987.

Iijima, T., and T. A. Potemra, Field aligned currents in the dayside cusp observed by TRIAD, *J. Geophys. Res., 81*, 5971, 1976.

Iijima, T., and T. Shibaji, Global characteristics of northward IMF-associated (NBZ) field-aligned currents, *J. Geophys. Res., 89*, 2408, 1984.

Maezawa, K., Magnetospheric convection induced by positive and negative Z components of the interplanetary magnetic field: Quantitative analysis using polar cap magnetic records, *J. Geophys. Res., 81*, 2289, 1976.

Maynard, N. C., Structure in the dc and ac electric fields associated with the dayside cusp region, in *The Polar Cusp*, edited by J. A. Holtet and A. Egeland, p. 305, D. Reidel, Norwell, Mass., 1985.

Maynard, N. C., T. L. Aggson, E. M. Basinska, W. J. Burke, P. Craven, W. K. Peterson, M. Sugiura, and D. R. Weimer, Magnetospheric boundary dynamics: De-1 and DE-2 observations near the magnetopause and cusp, *J. Geophys. Res., 96*, 3505, 1991.

Mozer, F. S., Electric field evidence on the viscous interaction at the magnetopause, *Geophys. Res. Lett., 11*, 135, 1984.

Murphree, J. S., R. D. Elphinstone, D. Hearn, and L. L. Cogger, Large-scale high-latitude dayside auroral emissions, *J. Geophys. Res., 95*, 2345, 1990.

Newell, P. T., and C. -I. Meng, Mapping the dayside ionosphere to the magnetosphere according to particle precipitation characteristics, *Geophys. Res. Lett., 19*, 609, 1992.

Newell, P. T., and C. -I. Meng, Ionospheric projections of magnetospheric regions under low and high solar wind pressure conditions, *J. Geophys. Res., 99*, 273, 1994.

Newell, P. T., W. J. Burke, C. -I. Meng, E. R. Sanchez, and M. E. Greenspan, Identification and observation of plasma mantle flow at low altitude, *J. Geophys. Res., 96*, 21,013, 1991a.

Newell, P. T., W. J. Burke, E. R. Sanchez, C. -I. Meng, M. E. Greenspan, and C. R. Clauer, The low-latitude boundary layer and the boundary plasma sheet at low altitude: prenoon precipitation regions and convection reversal boundaries, *J. Geophys. Res., 96*, 35, 1991b.

Reiff, P. H., and J.L. Burch, IMF B_Y-dependent plasma flow and Birkeland currents in the dayside magnetosphere, 2, A global model for northward and southward IMF, *J. Geophys. Res., 90*, 1595, 1985.

Reiff, P. H. and R. A. Heelis, Four cells or two? Are four cells really necessary?, *J. Geophys. Res., 99*, 3955, 1994.

Reiff, P. H., J. L. Burch, and R. W. Spiro, Cusp proton signatures and the interplanetary magnetic field, *J. Geophys. Res., 85*, 5997, 1980.

Rich, F. J., and M. Hairston, Large-scale convection patterns observed by DMSP, *J. Geophys. Res., 99*, 3827, 1994.

Ruohoniemi, J. M., and R. A. Greenwald, Statistical patterns of high latitude convection obtained from Goose Bay HF radar observations, *J. Geophys. Res., 101*, 21,743, 1996.

Russell, C. T., The configuration of the magnetosphere, in *Critical Problems of Magnetospheric Physics*, edited by E. R. Dryer, p. 1, IUCSTP, Nat. Acad. of Sci., Washington, D. C., 1972.

Russell, C. T., R. C. Snare, J. D. Means, D. Pierce, D. Dearborn, M. Larson, G. Barr, and G. Le, The GGS/Polar magnetic field investigation, in *The Global Geospace Mission*, edited by C. T. Russell, p. 563, Kluwer Acad., Norwell, Mass., 1995.

Sandholt, P. E., Auroral electrodynamics at the cusp/cleft poleward boundary during northward interplanetary magnetic field, *Geophys. Res. Lett. 18*, 805, 1991.

Sandholt, P. E., C. J. Faruggia, M. Oieroset, P. Staunning, and S. W. H. Cowley, Auroral signature of lobe reconnection, *Geophys. Res. Lett. 23*, 1725, 1996.

Scudder, J., et al., HYDRA – A 3 dimensional electron and ion hot plasma instrument for the Polar spacecraft of the GGS mission, in *The Global Geospace Mission*, edited by C. T. Russell, p. 459, Kluwer Acad., Norwell, Mass., 1995.

Shelley, E. G., et al., The toroidal imaging ion mass spectrograph (TIMAS) for the Polar mission, in *The Global Geospace Mission*, edited by C. T. Russell, p. 497, Kluwer Acad., Norwell, Mass., 1995.

Siscoe, G. L., W. Lotko, P. H. Reiff, and B. U. Ö Sonnerup, A high-latitude, low-latitude boundary layer model of the convection current system, *J. Geophys. Res., 96*, 3487, 1991.

Smiddy, M., W. J. Burke, M. C. Kelley, N. A. Saflekos, M. S. Gussenhoven, D. A. Hardy, and F. J. Rich, Effects of high-latitude conductivity on observed convection electric fields and Birkeland currents, *J. Geophys. Res., 85*, 6811, 1980.

Tsyganenko, N. A., Effects of the solar wind conditions on the global magnetospheric configuration as deduced from data based field models, *Third International Conference on Substorms (ICS-3), Eur. Space Agency Spec. Publ., ESA SP-389*, 181, 1996.

Weimer, D. R., Models of high-latitude electric potentials derived with a least square error fit of spherical harmonic coefficients, *J. Geophys. Res., 100*, 19,595, 1995.

Weimer, D. R., A flexible, IMF dependent model of high latitude electric potentials having "space weather" applications, *Geophys. Res. Lett., 23*, 2549, 1996.

Winningham, J. D., J. L. Burch, N. Baker, V. A. Blevins and R. A. Hoffman, The low altitude plasma instrument (LAPI), *Space Sci. Instrum., 5*, 465, 1981.

W. J. Burke, Phillips Laboratory, 29 Randolph Road, Hanscom AFB, MA, 01731-3010. (e-mail: burke@plh.af.mil)

R. P. Lepping, Laboratory for Extraterrestrial Physics, Code 696, Goddard Space Flight Center, Greenbelt, MD 20771. (email: rpl@leprpl/1.gsfc.nasa.gov)

N. C. Maynard and D. R. Weimer, Mission Research Corporation, One Tara Boulevard, Suite 302, Nashua, NH 03062. (email: nmaynard@mrcnh.com; dweimer@mrcnh,com)

F. S. Mozer, Space Science Laboratory, University of California, Berkeley, CA, 94720. (email: fmozer@sunspot.ssl.berkeley.edu)

W. K. Peterson, Lockheed Martin Space Sciences Laboratory, 3251 Hanover Street, Palo Alto, CA 94304. (email: pete@space.lockheed.com)

C. T. Russell, Institute for Geophysics and Planetary Physics, University of California, Los Angeles, CA, 90049. (email: ctrussell@igpp.ucla.edu)

J. D. Scudder, Department of Space Physics and Astronomy, University of Iowa, Iowa City, IA, 52240. (email: jds@space-theory.physics.uiowa.edu)

(Received March 21, 1997; revised July 23, 1997; accepted August 7, 1997.)